Evaluation of black carbon semi-direct radiative effect in a climate model

Jiangnan Li,[1] Knut von Salzen,[1] Yiran Peng,[1] Hua Zhang,[2] and Xin-Zhong Liang[3]

Received 1 October 2012; revised 18 February 2013; accepted 11 March 2013; published 29 May 2013.

[1] The semi-direct effect of black carbon (BC) is studied by using a newly proposed optical property parameterization for cloud droplets with BC inclusions. Based on Atmospheric Model Intercomparison Project-type climate model simulations, it is found that the cloud amount can be either enhanced or reduced when BC is included in clouds. The decrease of the global annual mean total cloud amount is only about 0.023%. The 3-D cloud fraction distribution, however, shows larger changes which vary with latitude. A correlation between the changes of the cloud fraction and the vertical velocity is found. The cloud water path is mainly affected by low clouds and so the impact of BC on the cloud water path is particularly strong. It is shown that the BC above clouds tends to stabilize the atmosphere and enhance the cloud amount in the boundary layer. This can be used to explain the relationship between aerosol optical depth and cloud amount according to satellite data. For BC in clouds and above, the global annual mean enhancement of solar absorption is about 0.049 W m^{-2} and 0.57 W m^{-2}, respectively. The BC semi-direct radiative forcing is estimated by subtracting the BC direct forcing from the BC total radiative forcing. The global annual mean of BC direct forcing and semi-direct forcing at the top of the atmosphere are 0.264 W m^{-2} and 0.213 W m^{-2}, respectively.

Citation: Li, J., K. von Salzen, Y. Peng, H. Zhang, and X.-Z. Liang (2013), Evaluation of black carbon semi-direct radiative effect in a climate model, *J. Geophys. Res. Atmos.*, *118*, 4715–4728, doi:10.1002/jgrd.50327.

1. Introduction

[2] Black carbon (BC) aerosol is a strong absorber of solar energy in the atmosphere and thereby contributes to the direct radiative forcing. BC is also responsible for the indirect radiative forcing by acting as cloud condensation nuclei (CCN), which affect cloud microphysical processes and change cloud lifetimes. In addition, BC can also exert the so-called semi-direct effect, i.e., absorbing BC aerosols embedded in or near a cloud layer can heat the cloud layer and promote cloud evaporation [*Hansen et al.*, 1997].

[3] Black carbon particles are mostly hydrophobic when emitted. However, BC aerosols become hydrophilic as they age in the atmosphere [*Croft et al.*, 2005]. In a cloud layer, BC particles can exist inside cloud droplets or interstitially between cloud droplets. In most current climate models, the semi-direct effect is taken into account by assuming that BC particles reside interstitially between cloud droplets (called interstitial aerosol) [*Johnson*, 2004; *Wang*, 2004; *Chung and Seinfeld*, 2005; *Hansen et al.*, 2005; *Jacobson*, 2006; *Jones et al.*, 2007: *Hill and Dobbie*, 2008; *Yoshimori and Broccoli*, 2008; *Zhang and Wang*, 2009; *Perlwitz and Miller*, 2010]. A review on the BC semi-direct effect is given in *Koch and Del Genio* [2010]. Some climate models [*Chuang et al.*, 2002; *Zhuang et al.*, 2010] have considered the extra BC heating by BC particles residing in cloud droplets. However, the method they used in the calculation of the cloud optical properties due to BC in cloud droplets is based on highly simplifying assumptions. The objective here is to re-investigate the cloud semi-direct effect by accurately accounting for the extra BC heating in clouds from application of a newly proposed cloud optical property parameterization.

[4] Black carbon aerosols represent a relatively small portion of atmospheric aerosols (typically less than 20% of the total aerosol mass). However, different from other aerosol species, BC has a relatively large imaginary part of the refractive index in the UV and visible range. Thus, BC strongly absorbs solar radiation because a substantial portion of solar incoming energy is within the UV and visible range. In Figure 1, the imaginary parts of refractive indices for BC, ammonium sulfate, and water are shown. This illustrates that the refractive index of ammonium sulfate is close to that of water. In a cloud droplet, since the volume ratio of aerosol is generally several to tens of order of magnitude smaller than that of water, contributions of ammonium sulfate and other

[1]Canadian Centre For Climate Modelling and Analysis, Science and Technology Branch, Environment Canada, Victoria, British Columbia, Canada.
[2]Laboratory for Climate Studies, National Climate Center, China Meteorological Administration, Beijing, China.
[3]Department of Atmospheric and Oceanic Science, University of Maryland, College Park, Maryland, USA.

Corresponding author: J. Li, Canadian Centre For Climate Modelling and Analysis, Science and Technology Branch, Environment Canada, Victoria, BC V8W 2Y2, Canada. (jiangnan.li@ec.gc.ca)

©2013. American Geophysical Union. All Rights Reserved.
2169-897X/13/10.1002/jgrd.50327

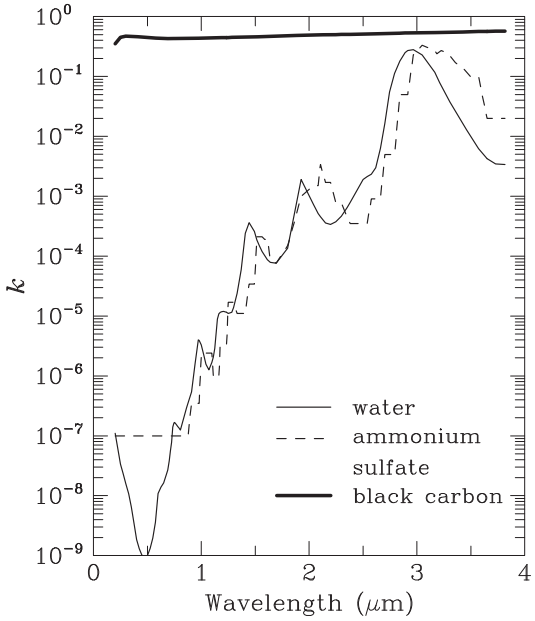

Figure 1. The imaginary part, *k*, versus wavelength for BC, ammonium sulfate, and water.

types of aerosol such as sea salt and dust to absorption in cloud droplets are negligible. However, the imaginary part of refractive index of BC is several to tens of order of magnitude larger than that of water. Thus, the impact of BC on cloud absorption is potentially important.

[5] Generally the cloud absorption is much stronger for BC inclusions in cloud droplets compared to interstitial BC. *Chylek et al.* [1996] found that the absorption of BC within a cloud droplet was increased by a factor of 2–2.5 at 0.55 μm. In Figure 2, the extra cloud solar heating rate by BC cloud inclusions is evaluated by using a single-column radiation model [*Li and Barker*, 2005]. For the calculation, a low cloud is assumed between 822 and 917 hPa with a liquid water content of 0.2 g m^{-}3 and a BC mass mixing ratio of 10^{-9} kg kg^{-1}. The atmospheric profile is representative of conditions during midlatitude summer over land. Two cases are considered: First, all the BC particles are included in cloud droplets, and second, all the BC particles are interstitial. For the former case, cloud optical properties are calculated based on *Li et al.* [2011]. For the latter, the cloud optical properties are calculated based on the method [*Briegleb*, 1992]. Figure 2 shows that the cloud heating rate by BC inclusions is about 2.5 times larger than that by the interstitial BC. Similar results are found for other clouds with different liquid water contents, solar zenith angles, and heights (results are not shown). The factor of 2.5 seems very robust. Therefore, an accurate treatment of BC in clouds, inside or interstitially between cloud droplets, is necessary in order to avoid underestimates of BC radiative effect in climate models.

[6] In current climate models, cloud optical properties are calculated by assuming pure water cloud droplets. A new parameterization has to be introduced by including the extra absorption due to the presence of BC in cloud droplets. Such an approach was first developed by *Chuang et al.* [2002], which included a parameterization of cloud single-scattering albedo with an explicit dependence on the in-cloud BC volume fraction. However, as pointed by *Li et al.* [2011], such parameterization was deficient in several aspects: (1) The effective radius should be used as the dependent variable instead of individual droplet sizes to more accurately capture properties of an ensemble of cloud droplets with different sizes; (2) Mie calculations, instead of an empirical formula, should be use to obtain the parameterization for cloud optical properties. Empirical methods can produce errors in absorption by up to 30% compared to Mie calculation results. (3) Under certain conditions, the asymmetry factor should be considered to avoid an inconsistency in cloud optical properties.

[7] *Li et al.* [2011] proposed a new parameterization scheme for water cloud optical properties with presence of BC in cloud droplets which addresses these concerns. The new scheme uses the perturbation technology to account for the BC effect. The approach has the advantage for climate models that it can be easily combined with existing radiation parameterizations for pure water clouds. Changes of cloud optical properties due to BC inclusions in cloud droplets are conceptually treated as a perturbation in radiation parameterizations.

[8] In this work, the above mentioned parameterization is included in a comprehensive global climate model. In section 2, influences of BC aerosol on simulated cloud properties, such as cloud amount, liquid water content, and atmospheric instability are investigated. The impact of BC heating on the radiative absorption and on global radiative energy balance is shown in section 3. In section 4,

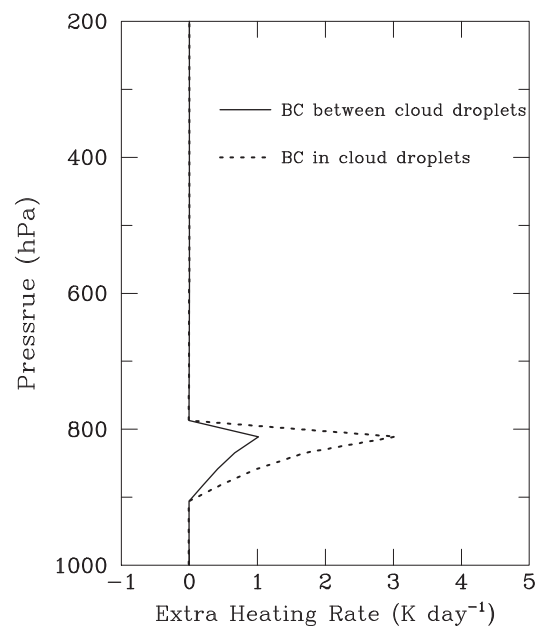

Figure 2. The extra cloud solar heating rates due to the presence of BC in clouds, by assuming that all BC particles are interstitially existing between cloud droplets (solid line) and all BC particle are existing in cloud droplets (dashed line). The atmospheric profile is midlatitude summer with solar zenith angle 60°. The cloud liquid water content is 0.2 g m^{-3}, and the BC mixing ratio is 10^{-9} kg kg^{-1}.

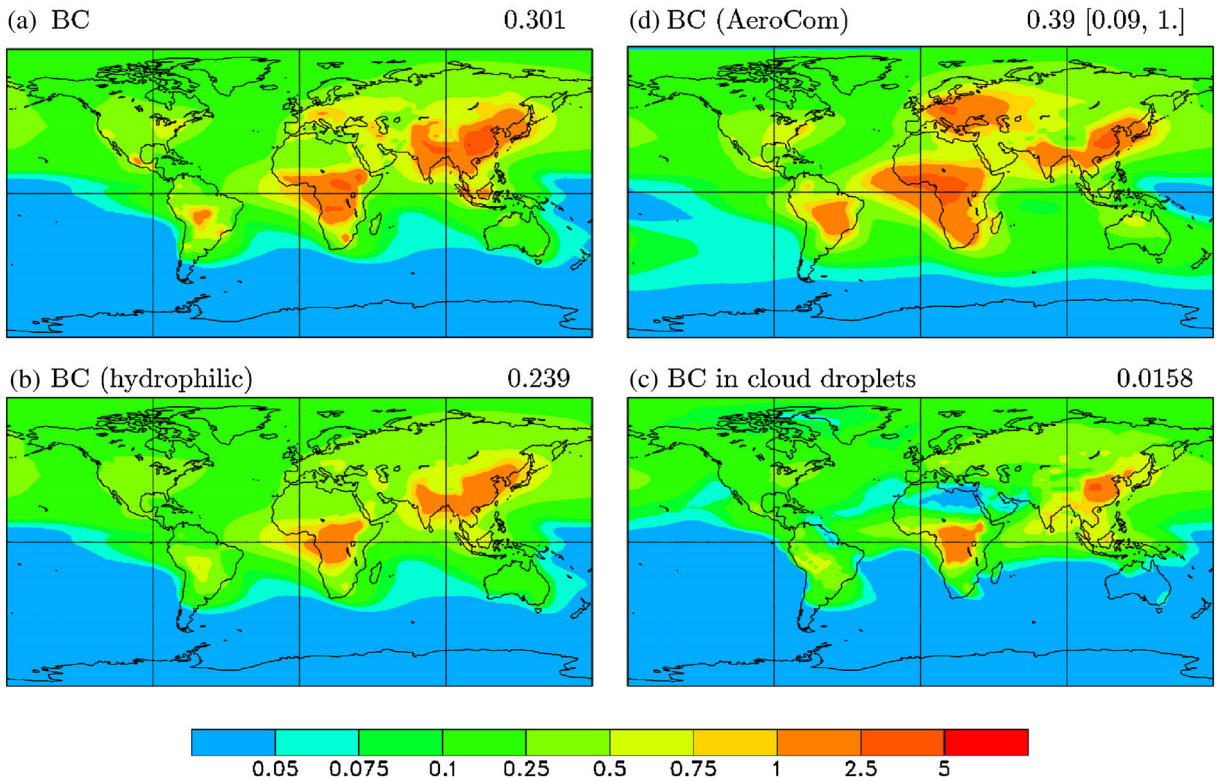

Figure 3. The loading distributions of (a) total BC, (b) hydrophilic BC, (c) BC in cloud droplets, and the (d) mean result of BC from AeroCom. The scale units are 0.1 mg m^{-2} for the loading of BC in cloud droplets (Figure 3c) and mg m^{-2} for Figures 3a, 3b, and 3d. The numbers shown on each panel are the global mean values in units mg m^{-2}.

the semi-direct radiative forcing of BC aerosol is estimated and analyzed. In section 5, we conclude with a brief summary.

2. Impact of BC Aerosol on Cloud Fraction and Liquid Water Content

[9] Black carbon aerosol particles are mostly located in the lower troposphere, and the volume fraction of BC inside ice clouds is very small. Therefore, the proposed parameterization for BC in cloud droplets is only applied to water clouds.

[10] The model used here is the fourth generation of the Atmospheric Global Climate Model of the Canadian Centre for Climate Modelling and Analysis, CanAM4, [*von Salzen et al.*, 2013], which employs a spectral resolution of T63, with 35 vertical levels from the surface up to 1 hPa. The model includes prognostic parameterizations for BC aerosol mass concentrations and produces good agreement between model results and observations [*Croft et al.*, 2005]. In Figure 3, the simulated BC mass loading from CanAM4 is compared to a multi-model estimate from the AeroCom (Aerosol Comparison between Observations and Models) project based on simulations with 12 different global models (http://aerocom.met.no/). Simulations are based on climate conditions in year 2000. Simulations with CanAM4 are based on emissions from the fifth Coupled Model Intercomparison project, CMIP5 (K. Taylor et al., A summary of the CMIP5 experiment design, unpublished CMIP5 internal document, pp. 33, 2011, http://cmip644pcmdi.llnl.gov/cmip5/docs/TaylorCMIP5design.pdf), whereas slightly different emissions were used in the AeroCom models [*Dentener et al.*, 2006]. The global mean BC loading estimated from AeroCom varies between 0.09 and 1 mg m^{-2} for different models, with a median value of 0.39 mg m^{-2}. The global mean BC loading from CanAM4 is 0.30 mg m^{-2}, which is within the range of AeroCom results. The pattern of BC loading in CanAM4 is similar to that of the multi-model estimate from AeroCom. The most noticeable difference is that CanAM4 tends to produce relatively low BC loadings in major source regions of Central Africa and Europe compared to the AeroCom median.

[11] Given that only hydrophilic BC is considered in the calculation of BC inclusions in cloud droplets, the distribution of mass loading for hydrophilic BC is also shown in Figure 3b. The global mean loading of hydrophilic BC is 0.239 mg m^{-2}. Thus about 79% BC particles are hydrophilic in CanAM4.

[12] A comparison between simulated near-surface BC mass concentrations with measurements at 196 sites from different networks during the time period of the simulation is shown in Figure 4. The IMPROVE (Interagency Monitoring of Protected Visual Environments) monitoring network consists of aerosol, light scatter, light extinction, and scene samplers in a number of national parks and wilderness areas in the United States. Aerosol samples are collected on a quartz filter and are analyzed for elemental carbon using the thermal optical reflectance combustion

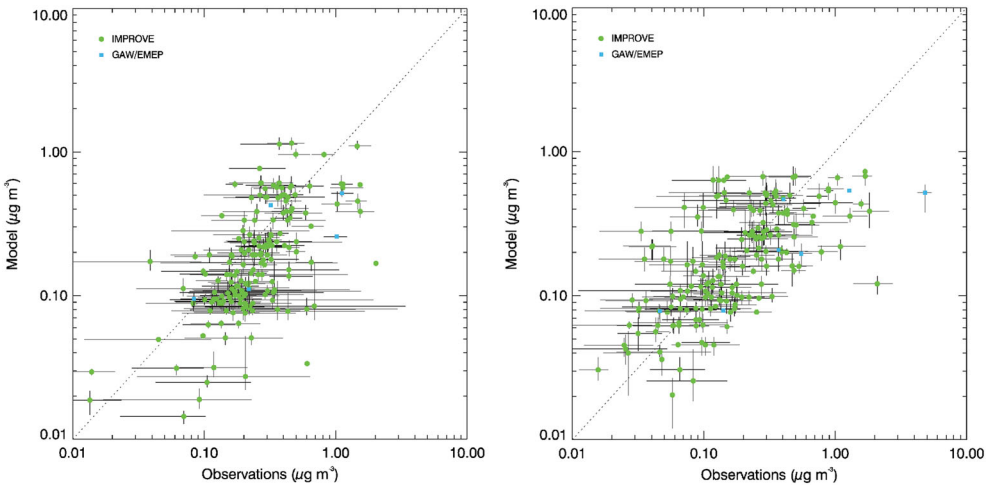

Figure 4. Simulated and observed near-surface concentrations of black carbon for June to August and December to February. Mean results during the time period of the simulation (symbols) and their ranges are shown based on monthly mean data from model and observations. For the model results, grid points nearest to the sites of the observations were selected. Circles correspond to data from the Interagency Monitoring of Protected Visual Environments (IMPROVE, http://vista.cira.colostate.edu/improve/) network and squares to data for European and Arctic sites from the Global Atmospheric Watch (GAW, http://gaw.empa.ch/gawsis/) and the European Monitoring and Evaluation Programme (EMEP, www.emep.int; *Torseth et al.* [2012]) data bases.

method. Aethalometer-based measurements of black carbon from the Global Atmospheric Watch (GAW) and the European Monitoring and Evaluation Programme (EMEP) data bases are available at seven surface sites in Europe and the Arctic, including Alert (82.50°N, 62.34°W) and Hyytiälä (61.85°N, 24.29°E). According to results shown in Figure 4, the magnitudes of the simulated and observed BC concentrations agree reasonably well at most of these sites. On average, concentrations are slightly underestimated in the simulation (–25% for JJA and –21% for DJF). This could be caused by various factors including uncertainties in emissions, dry and wet deposition, and aerosol aging processes. Similar biases are found for other models in an analysis of model data from CMIP5 (Taylor et al., unpublished document, 2011) and other global aerosol models [*Bond et al.*, 2013].

[13] In order to account for the effects of BC on cloud optical properties, the volume fraction of BC to cloud water is given [*Li et al.*, 2011]

$$\eta = f_c \frac{f_a m_{\mathrm{bc(y)}}}{m_{\mathrm{w}}} \frac{\rho_{\mathrm{w}}}{\rho_{\mathrm{bc(y)}}},$$

where f_c is the cloud fraction in a model grid cell, $m_{\mathrm{bc(y)}}$ and m_{w} are grid-mean mass mixing ratios of hydrophilic BC and cloud liquid water, $\rho_{\mathrm{bc(y)}}$ and ρ_{w} are densities of hydrophilic BC and cloud liquid water, m_{w}/f_c is the cloud-mean mass mixing ratios of cloud liquid water. A factor of f_a is added. It represents the mass fraction of total hydrophilic BC, which resides inside the cloud droplets in the cloudy part of the grid cell. Owing to efficient activation of hydrophilic aerosol and collision/coalescence processes in clouds, only a relatively small fraction of the aerosol is partitioned outside of the cloud droplets as interstitial aerosol. Simulations of microphysical processes in clouds yield values of f_a that are in the range of 0.8–0.9 [*Flossmann*, 1998; *Flossmann and Wobrock*, 2010]. For this study, 0.85 is chosen. The dependency of f_a on the size and chemical composition of the aerosol is beyond the scope of this study and will be addressed in the future based on detailed simulations of aerosol and cloud microphysical processes.

[14] In contrast to hydrophilic BC, hydrophobic BC does not contribute to BC inclusions in cloud droplets. Consequently, the mass mixing ratio of interstitial BC is given by

$$(1 - f_a) m_{\mathrm{bc(y)}} + m_{\mathrm{bc(o)}},$$

where $m_{\mathrm{bc(o)}}$ is the mass mixing ratio of hydrophobic BC. Finally, the BC mass mixing ratio in the clear-sky portion of a grid cell is given by

$$(1 - f_c)(m_{\mathrm{bc(y)}} + m_{\mathrm{bc(o)}}).$$

[15] The vertical integrated loading of the hydrophilic BC embedded in cloud droplets can be obtained by

$$\frac{1}{\mathrm{g}} \int_{p_s}^{p_t} f_c f_a m_{\mathrm{bc(y)}} \, \mathrm{d}p$$

where p is the pressure, p_s and p_t are the pressure at the surface and top of the atmosphere (TOA), respectively, and g is the gravitational acceleration. The loading distribution of BC inclusion in cloud droplets is shown in Figure 3c. The global mean loading of BC inclusions in cloud droplets is 0.0158 mg m^{-2}. This indicates that about 5.2% of all BC particles are included in cloud droplets. The loading distribution of BC in cloud droplets is different from that of the hydrophilic BC, especially in subtropical regions. This is because the cloud fraction is very low in these regions.

[16] In CanAM4 and several other global climate models (GCMs), an empirical relationship between sulfate aerosol concentration and cloud droplet number concentration is used [*von Salzen et al.*, 2013], without explicit calculation of

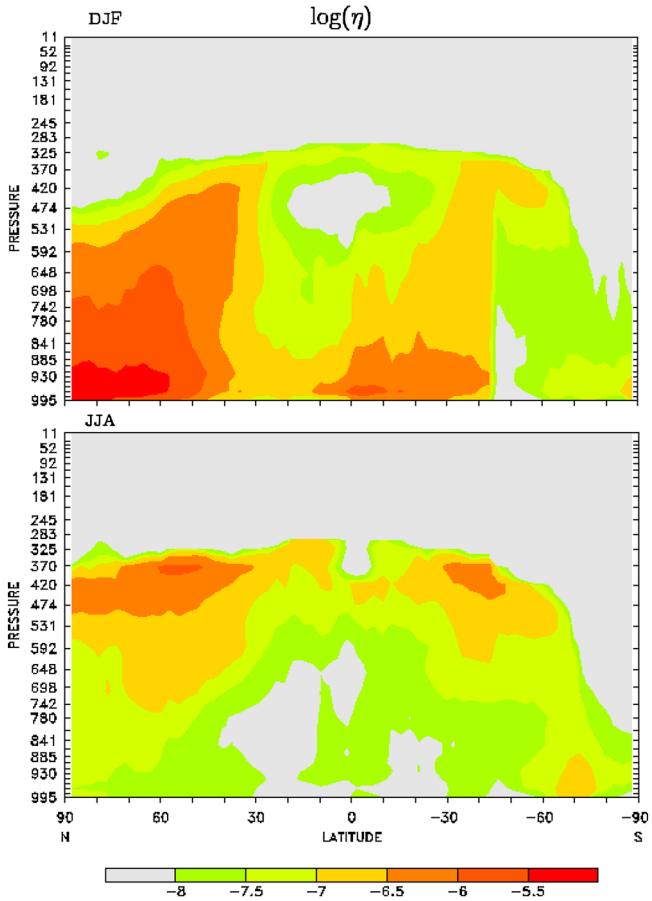

Figure 5. The zonally distributions of the volume fraction of black carbon in cloud droplet (η) in DJF and JJA seasons. η is in logarithm scale.

the activation of CCN to cloud droplets. In reality, CCN activate and form cloud droplets if the supersaturation exceeds a critical value that can be predicted by Köhler theory based on the size and chemical composition of the aerosol. This is the first principle in the physical evolution of cloud droplets from aerosol particles and has been applied to some climate models [for example, *Gustafson et al.* 2008 and *Ghan et al.* 2012]. In these models, the number of aerosols entering cloud droplets, including BC, is calculated explicitly. According to *Ghan et al.* [2012], about 3% of the simulated BC is cloud borne, which is slightly smaller than 5.2% obtained here. Differences in the spatial and temporal distributions of clouds and aerosols between different models are substantial [*Koch et al.*, 2009] and very likely contribute to differences in simulated amounts of BC inclusions in cloud droplets.

[17] In *Li et al.* [2011], it is shown that the radiative forcing is sensitive to the value of η. In Figure 5, the zonal and 10 year mean BC volume fraction in CanAM4 is shown. The result is a cloud fraction weighted average which only includes points where clouds are present. In the winter season, large values of η occur at high latitudes in the Northern Hemisphere where emissions or BC are high compared to other regions. A low cloud water content under cold and dry conditions may also contribute to a high η. This may explain the maximum which appears in the Arctic in winter and spring. A second region with high values of η in the Tropics is attributed to the emission of BC from biomass burning in central Africa (see Figure 3). However, the high cloud water content from the tropical clouds tends to dilute the concentrations of BC inclusions in clouds so that values of η are relatively low. In the summer time, η becomes small in the lower troposphere because more cloud water in this season dilutes the BC concentrations. In contrast, the high η in the upper troposphere is mainly due to the low cloud water content. The concentrations of BC are much lower in the summer Arctic because the insufficient transport of BC to the Arctic as the polar dome is smaller in the summer. Also, wet deposition is greater in the summer. Therefore, η becomes much lower in the summer in the Arctic. It is seen that η is mostly within the range between 10^{-8} and 10^{-6}. Based on the offline results estimated in *Li et al.* [2011], these values of η may result in a local radiative forcing roughly in the range of 0.02–2 W m^{-2}, without considering climate feedbacks.

[18] We first investigate the impacts of BC inclusions in cloud droplets on simulated climate. The simulation is forced by CMIP5 sea surface temperatures and sea ice extent averaged over the period of 1999–2009. Eleven-year climate integrations were performed with model spin-up of 1 year. Results from the 10 years of the simulation are averaged in order to minimize effects of natural variability in the results.

[19] Two GCM experiments were performed: in the first, a f_a portion of the hydrophilic BC is included in the liquid cloud droplets. The remainder and the hydrophobic BC are interstitial between cloud droplets. None of the BC in the clouds is assumed to be radiatively active. Only the BC in the clear-sky portion of the grid cells is radiatively active in the simulation (hereafter referred to as NOCL). In the second, all types of BC aerosol are radiatively active in the clouds and in the clear-sky in the simulation (referred to as STAD). All other calculations of cloud optical properties are the same for the two experiments. The parameterization of *Baumer et al.* [2007] is applied to obtain the BC aerosol optical properties and radiative effects under clear-sky conditions in both simulations.

[20] Figure 6 shows the differences in the total cloud amount and cloud fraction distribution between STAD and NOCL (STAD-NOCL). The total cloud amount is the cloud fraction as viewed from the TOA. The overlap of adjacent and nonadjacent cloud layers is properly accounted for in the calculation of total cloud amount in CanAM4. It is based on a combination of maximum and random overlap by using the decorrelation length approach [*Räisänen et al.*, 2004]. In the following, we denote the total cloud amount as CLDT. It is seen in Figure 6 (top row) that differences in CLDT are more obvious in the Northern Hemisphere during DJF (December to February) and JJA (June to August). Results also indicate that the local variation of CLDT, due to BC inclusions in clouds droplets, can be either positive or negative. The cloud amount depends on many physical factors so that effects from the heating from BC aerosols are nontrivial. The two-tailed approximate t test is used to examine the reliability of the result shown in Figure 6. The nonsignificant cells of confidence level under 95% are shown in white. A large fraction of the model domain does not pass this confidence level.

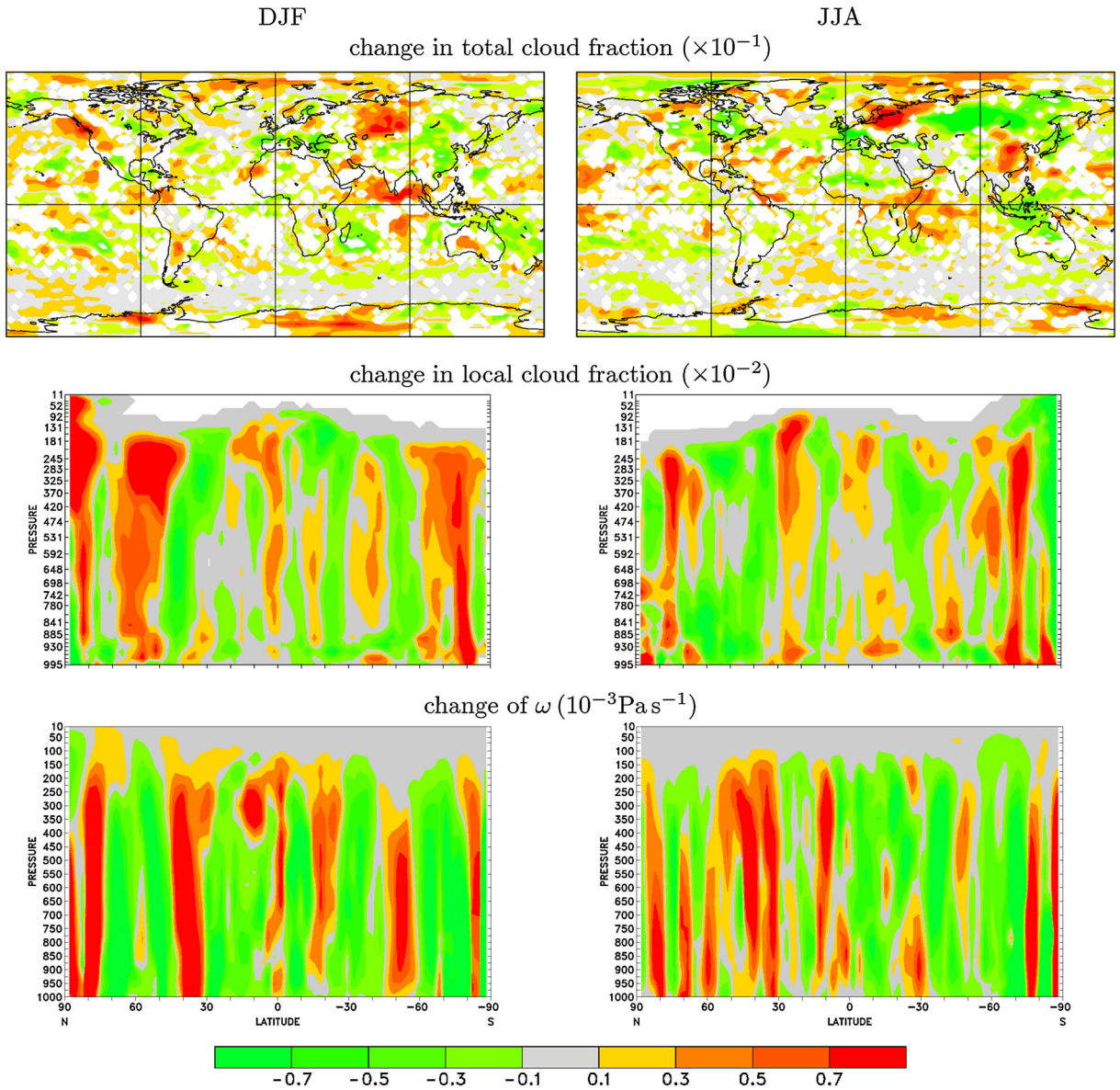

Figure 6. (top row) The global distributions of the changes in total cloud amount by STAD-NOCL, with two seasons of DJF and JJA; (middle row) the corresponding zonal mean distributions of the local cloud fraction; and (bottom row) the zonal mean change of the vertical velocity.

[21] Table 1 shows the results of the change in CLDT for global and hemispheric means. The global annual mean change in CLDT is about –0.00143. Since the global mean total cloud amount is about 0.6, the cloud amount is reduced by only about 0.24%. It is seen in Table 1 that the reduction in CLDT in JJA is about three times larger in the Northern Hemisphere than in the Southern Hemisphere, which is likely explained by higher BC loadings in the Northern Hemisphere.

Table 1. The Differences in Cloud Fraction (CLDT; $\times 10^{-3}$) and Liquid Water Path (CLWP; in Units of 10^{-1}kg m^{-2})[a]

	STAD-NOCL			STAD-NOUP		
	Globe	North	South	Globe	North	South
CLDT	–1.43	–0.838	–0.267	–0.323	1.28	0.429
		–3.133	0.502		–0.334	0.836
CLWP	–0.281	0.066	–0.277	–0.077	0.503	0.0413
		–0.796	–0.036		–0.289	0.102

[a]The data in "Globe" are the global annual mean results; the data in "North" (South) are the northern (southern) hemispheric (first row) DJF and (second row) JJA mean results.

[22] Though the global mean reduction in CLDT is small, the local change in CLDT can be considerably larger. In JJA, the reduction in CLDT in the central Siberian Plateau is up to 0.1. Thus, the change in cloud amount is over 10%. However, in such regions the local BC loading is low (see Figure 3). Therefore, the simple correlation between BC loading and the reduction in cloud amount does not exist. The correlation coefficient between CLDT and vertical BC loading was calculated. In most regions, the correlation coefficient is in the range of –0.3 to 0.3. *Koch and Del Genio* [2010] showed that simulated cloud amount changes in response to BC aerosol are very different for different

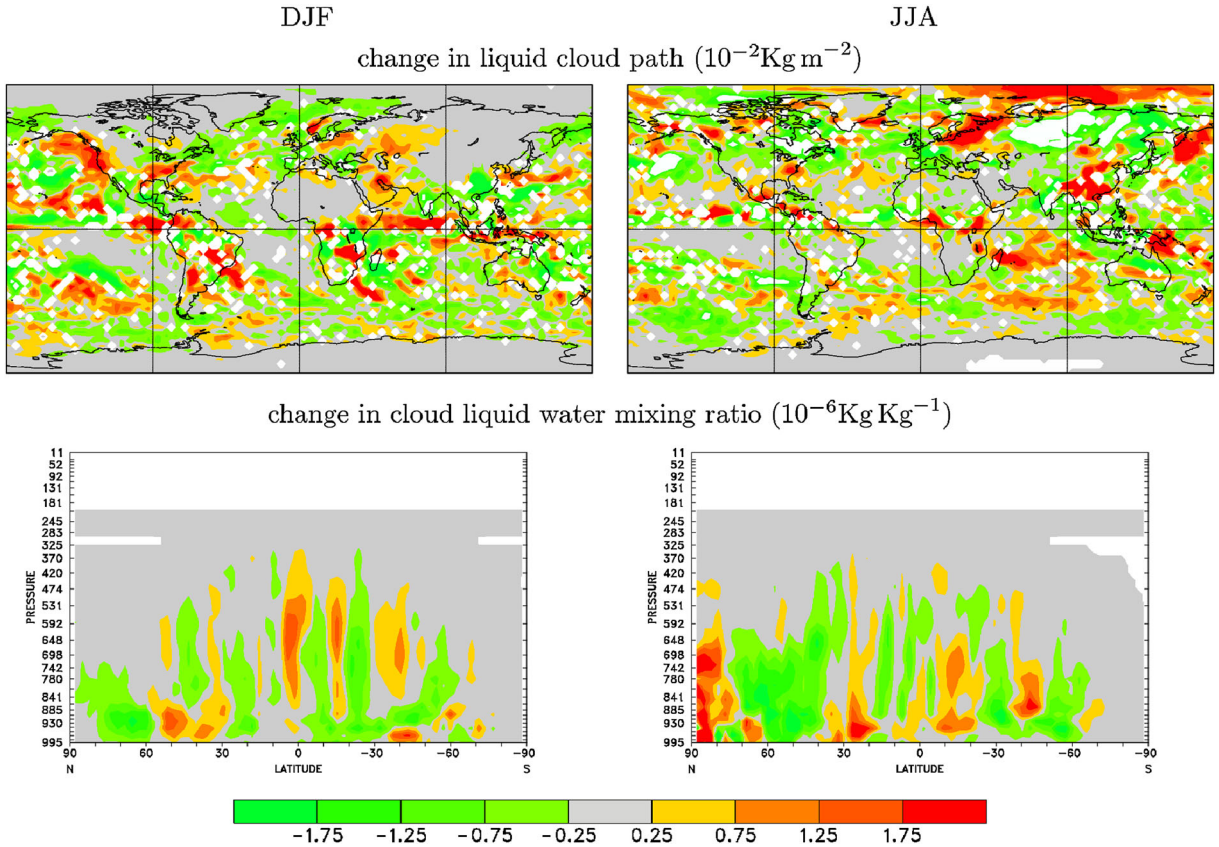

Figure 7. (top row) The global distributions of the cloud liquid water path for DJF and JJA; (bottom row) the corresponding zonal mean distributions of cloud liquid water mixing ratio.

models. Simulated changes generally produce poor agreement with observations. For instance, *Brioude et al.* [2009] have studied the change in stratocumulus cloud amount near the coast of California by comparing observational data for clean versus polluted (in terms of biomass burning) continental air masses. Biomass burning aerosols tend to reside above the marine boundary layer, which caused an increase in cloud fraction by 0.143. Using satellite data over the Amazon region during the biomass burning season, *Koren et al.* [2004] showed that scattered cumulus cloud cover was reduced by 38%.

[23] As mentioned above, the calculation of CLDT in a grid cell depends on the overlap of different cloud layers in the atmosphere. High (ice) clouds contribute strongly to CLDT in tropical and extratropical regions. In order to better understand changes in cloud structure, the height-dependent cloud fraction is shown in Figure 6. In Figure 6 (middle row), the zonal mean vertical distribution of the change in cloud fraction is shown. In the Northern Hemisphere, the reduction of cloud amount is considerably larger in JJA, compared to DJF, especially at higher latitudes.

[24] In the Northern Hemisphere from 30°N to 70°N in JJA, a region with a large decrease in cloud amount is apparent, corresponding to results in the central Siberian Plateau and North America as shown in Figure 6 (top row). In the Arctic in winter, there are large decreases in the amounts of water clouds in the lower troposphere and large increases in the amount of ice clouds in the upper troposphere. Thus, CLDT increases in this region. This change in high clouds is not directly associated with the in-cloud BC heating.

[25] The zonal mean distributions in Figure 6 show that the change in cloud fraction is regionally variable. The cloud fraction generally increases in regions of large-scale ascent. In these regions, the extra BC heating can enhance the upward air motion and cause more vigorous upward transport of moisture which then leads to the formation of more clouds. At the same time, the extra heating in clouds exacerbates cloud evaporation. The net effect on cloud fraction depends on the competition of these two factors. Similarly, the extra heat weakens the subsidence in subtropical regions which leads to an increase in the cloud fraction there.

[26] In order to verify the correlation between the cloud fraction and vertical motions, in Figure 6 (bottom row), we analyze the zonal mean distributions of the change in vertical velocity ($\omega = dp/dt$). It is seen that the changes in cloud fraction and vertical velocity are well correlated. Generally, an enhanced cloud fraction is associated with an increase in upward air motion. Therefore, in regions of strong correlation between the cloud fraction and vertical velocity, the change in cloud fraction is more associated with the atmospheric instability caused by the extra heating of BC. In the regions of weak correlation between the cloud fraction and vertical velocity, the change in cloud fraction is more associated with the direct cloud burn-off that results from the extra in-cloud BC heating. We will further address this in the discussion of Figure 8.

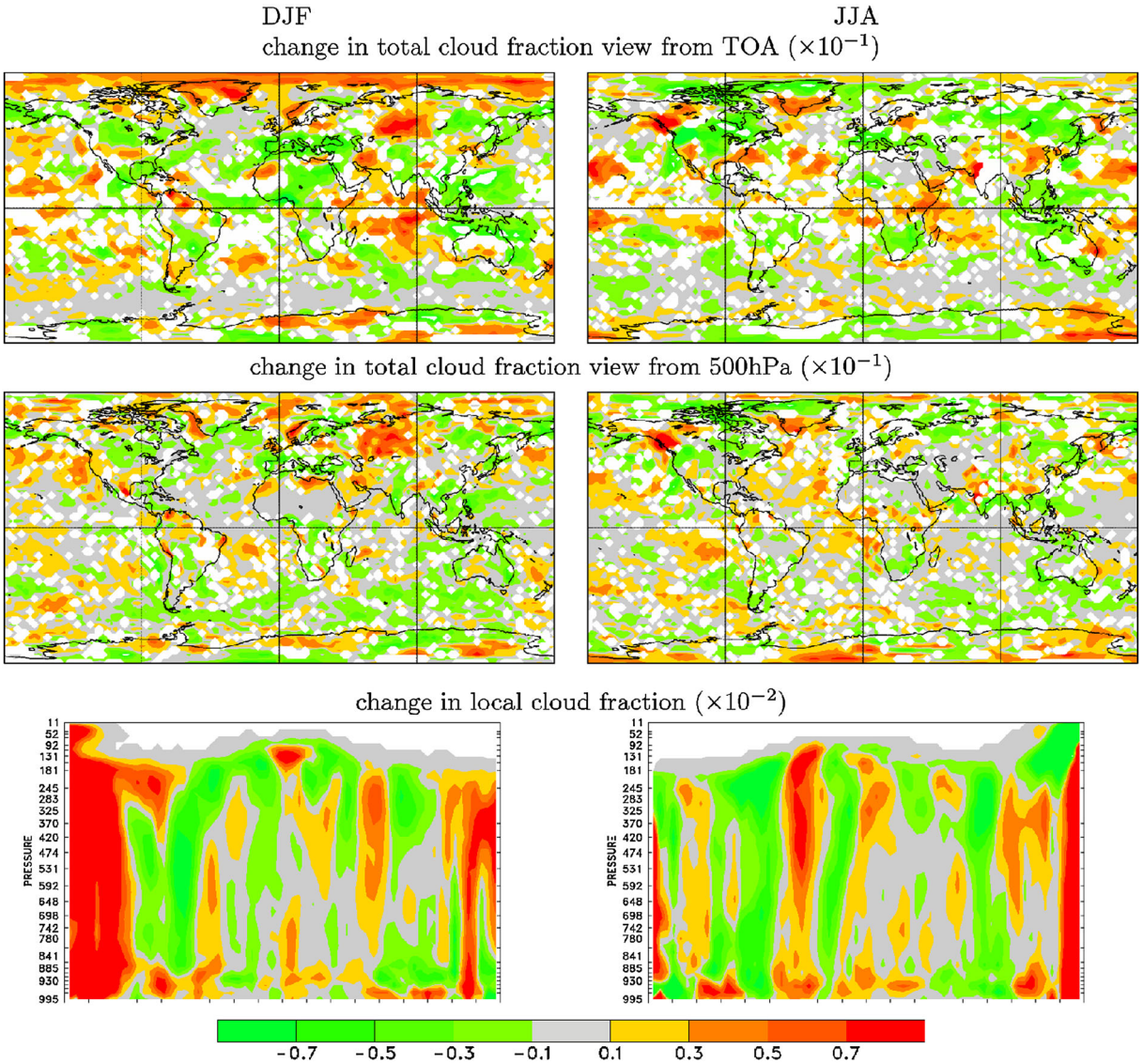

Figure 8. The global distributions of the changes in total cloud amount by STAD-NOUP viewing from (top row) TOA and (middle row) 500 hPa; (bottom row) the results of the zonal mean distributions of the local cloud fraction.

[27] *Hill and Dobbie* [2008] used a large eddy simulation model to study the impact of absorbing aerosols on marine stratocumulus. They found that BC aerosol generally reduces the cloud liquid water path which leads to a positive semi-direct effect. In Figure 7 (top row), the global distributions of the change in cloud liquid water path (CLWP) are shown for STAD-NOCL. By comparing to results in Figure 6, it is apparent that the global distributions of changes in CLWP are generally correlated with changes in CLDT. For example, in JJA large positive values appear in the central Siberian Plateau for both CLDT and CLWP. Since CLWP is only very weakly related to high clouds, changes in CLWP are related to the in-cloud BC heating effect. This is verified as the nonsignificant area of confidence level of less than 95% is reduced in comparison with the results shown in Figure 6. In Figure 7 (top row), it is apparent that changes in CLWP mostly occur in the Tropics and at midlatitudes. This supports our point that changes in clouds are related to changes in atmospheric circulation.

[28] In Figure 7 (bottom row), zonal mean distributions of the cloud liquid water mixing ratio are shown. Considering the regions below 400 hPa, changes in cloud liquid water mixing ratio are similar to results for cloud fraction shown in Figure 6 (middle row). Therefore, different responses in CLDT and CLWP are mostly related to ice clouds at higher altitudes.

[29] In Table 1, changes in CLWP are listed. In the global and annual mean, changes in CLWP are negative, which is consistent with changes in CLDT. However, seasonally averaged changes in CLWP in the Northern and Southern Hemispheres are not always similar to changes in CLDT. For example, in the DJF Northern Hemisphere and JJA Southern Hemisphere, CLWP changes are of opposite sign than those of CLDT, similar to changes in cloud fraction. This is particularly true in the Southern Hemisphere, where BC

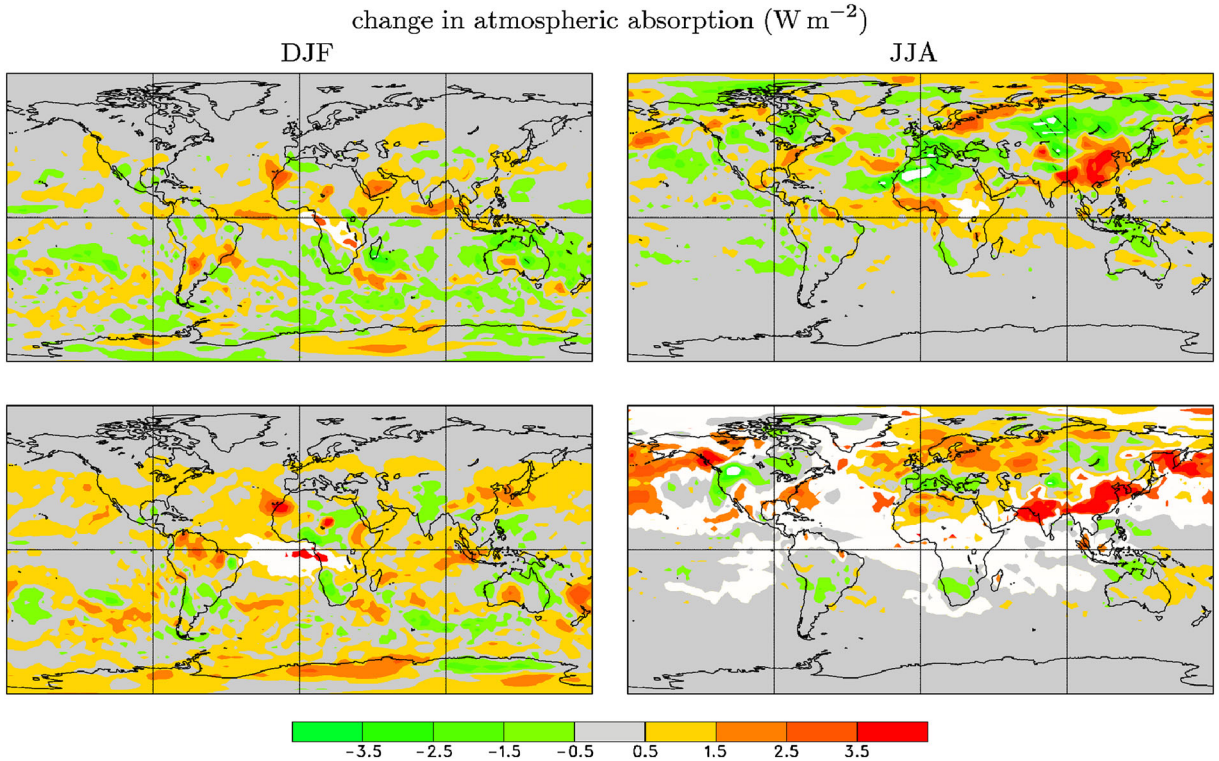

Figure 9. Differences in atmospheric absorption for (top row) STAD-NOCL and (bottom row) STAD-NOUP.

heating effects are small and circulation feedbacks play an important role.

[30] According to the review by *Koch and Del Genio* [2010], radiative heating from BC aerosol above clouds can stabilize the atmosphere. BC located above clouds may therefore lead to an increased cloud cover. However, most of the previous studies are based on large eddy simulation models or cloud resolving models. Results from GCMs have not been analyzed in detail before.

[31] Based on STAD, another 11 year climate integration was performed in which the BC particles are not assumed to be radiatively active above the liquid water clouds. In each model grid cell, the optical depth of BC is set to zero above the highest water cloud layer. Otherwise, the model approach is the same as for STAD. We refer to this GCM simulation as NOUP.

[32] In Figure 8 (bottom row), zonal mean distributions of the change in cloud fraction are shown for STAD-NOUP. In STAD-NOUP, the solar absorption above water clouds is strongly enhanced (see Figure 9), which stabilizes the atmosphere by suppressing upward air motions. The cloud fraction is most strongly influenced by the humidity and lower tropospheric stability. The increase in lower tropospheric stability can enhance the boundary cloud fraction [*Koch and Del Genio*, 2010]. This is confirmed by observations [*Brioude et al.*, 2009]. Furthermore, results shown in Figure 8 indicate that the stabilization effect leads an enhancement in boundary cloud fraction. Results shown in Figure 8 (bottom row) are very different from those in Figure 6 (middle row). The latter does not show an obvious change in boundary cloud fraction. The in-cloud extra BC heating causes a more efficient upward transport of water vapor into the mid-troposphere which leads to a change in cloud fraction there.

[33] Table 1 lists the changes in CLDT for STAD-NOUP. Global annual mean changes in CLDT are negative but very small. For seasonally averaged hemispheric means, both positive and negative changes are found. The maximum increase in cloud amount occurs in the Northern Hemisphere in DJF. This is due to the increase in amounts of boundary layer clouds as shown in Figure 8 (bottom row).

[34] Relationships between aerosol optical depth (AOD) and cloud amounts (CLDT) have been previously analyzed by *Koren et al.* [2004] and *Ten Hoeve et al.* [2011]. According to these studies, an increase in CLDT is associated with an increasing AOD at a low AOD. However, CLDT decreases with increasing AOD at a high AOD. This demonstrates that the cause and effect relationship between AOD and CLDT is complicated. We speculate that warming effects from BC may explain part of the observed relationships. When the AOD is relatively low, the warming effect due to aerosol (especially for BC) inside or near clouds may cause the clouds to burn off according to the semi-direct effect. This would cause CLDT to decrease with increasing amounts of aerosol and therefore AOD. Since the aerosol concentration decreases with height in a quasi-exponential manner, a low aerosol loading is generally associated with lower aerosol concentrations above cloud. However, when AOD becomes relatively large, concentrations of aerosols above boundary layer clouds also become large. For BC, as discussed above, extra heating above boundary layer cloud tends to stabilize the atmosphere and enhances the cloud amount in the boundary layer. For other types of aerosol, the extra AOD above the water clouds produces a larger

scattering effect and therefore causes less solar radiation to reach the cloud top. This leads to less cancelation between shortwave warming and longwave cooling at cloud top. The extra longwave cooling at cloud top can further enhance the cloud fraction.

[35] In this work, though we only focus on BC, the hypothesis presented above can be partly tested. Figure 8 (top row) shows differences in total cloud amount distribution between STAD and NOUP (STAD-NOUP). It is seen that changes in CLDT are more obvious in the Northern Hemisphere, especially in JJA. In regions with high BC loading such as southeastern Asia, western Europe, and central Africa, changes in CLDT are generally positive. In the other regions, like central United States, eastern Russia, and south Latin America, changes in CLDT are generally negative. This supports the AOD-CLDT relation according to the analysis of satellite data. In the Arctic in winter, changes in cloud amount are obviously positive. These changes may not be directly caused by warming from BC but may instead be related to the influence of high clouds. To confirm this point, in Figure 8 (middle row), we present differences in cloud amount distributions between STAD and NOUP for water clouds which occur below 500 hPa. The results show that the enhancement in cloud amount in the Arctic in winter is much reduced. There are also significant reductions in changes in the tropics. This indicates that changes in CLDT in the Arctic in winter and in the Tropics are mostly due to ice clouds. Results shown in Figure 8 (middle row) are similar to those in Figure 8 (top row) for all other regions. This indicates that changes in CLDT are mostly due to water clouds and are related to extra heating by BC.

[36] Results in Figure 8 demonstrate that changes in CLDT mostly depend on atmospheric stability and cloud burn-off from local warming. This explanation is supported by an analysis of satellite data [*Koren et al.*, 2004; *Ten Hoeve et al.*, 2011]. However, some regions produce a different AOD-CLDT relationship. For example, large positive changes in CLDT occur over Alaska in summer where the BC loading is low. The role of other types of aerosol is not analyzed in this study and may partly explain this discrepancy.

3. Impact of BC Heating on Radiation

[37] In this section, we further study the impact of BC heating on the radiative absorption and radiative energy balance at TOA and at the surface. In Figure 9, the vertically integrated atmospheric absorption (FSA) is shown for STAD-NOCL and STAD-NOUP.

[38] In STAD-NOCL, the change in atmospheric solar absorption is small in the Northern Hemisphere in DJF due to the low fluxes of incoming solar energy. However, the enhanced solar absorption in the JJA Northern Hemisphere is relatively large, with a maximum value about 4 W m^{-2} in eastern China. On the one hand, existing BC inclusions in cloud droplets can enhance the solar absorption directly. On the other hand, if the extra in-cloud BC heating causes clouds to burn off, then the atmospheric absorption will also be reduced. This is because a lower cloud fraction will lead to an increased flux of solar radiation at the surface, which then results in less solar absorption in the atmosphere. In JJA, a large increase in atmospheric absorption happens in southeastern Asia. In this region, the BC loading is relatively large. However, the large BC loading does not directly cause the cloud amount reductions in this region as shown in Figure 6. The existing BC above clouds can enhance the atmospheric absorption (see discussion for Figure 9, bottom row). In contrast, regions in the central Siberian Plateau, North Africa and in the Mediterranean give evidence for reductions in solar absorption. These regions, as shown in Figure 6, have experienced obvious cloud amount reductions and a large decrease of atmospheric absorption.

Table 2. The Same as Table 1, but for Atmospheric Solar Absorption (FSA), Solar Reflected Flux at TOA (FSR) (in Units of 10^{-1} W m^{-2})[a]

	STAD-NOCL			STAD-NOUP		
	Globe	North	South	Globe	North	South
FSA	0.485	0.944	0.302	5.17	3.59	4.52
		1.43	0.963		1.20	3.42
FSR	–2.57	–2.10	–3.19	–2.43	–1.54	–0.870
		–5.94	–0.107		–5.59	–0.451
FSG	2.08	1.05	2.59	–2.73	–2.15	–3.94
		4.51	–0.855		–6.49	–2.97

[a]The data in "Globe" are the global annual mean results; the data in "North" (South) are the northern (southern) hemispheric (first row) DJF and (second row) JJA mean results.

[39] Table 2 shows annual mean changes in solar absorption. For STAD-NOCL, the changes in atmospheric absorption are all positive for global and hemispheric means.

[40] Figure 9 (bottom row) shows changes in solar absorption for STAD-NOUP. The increase in solar absorption in the Northern Hemisphere is relatively large, with changes of over 1.5 W m^{-2} for most regions. In southeastern China and western central Africa, the enhancement in atmospheric absorption is over 4 W m^{-2}, which is consistent with the large BC loading in these regions as shown in Figure 3. Increases in solar absorption in the Northern Hemisphere in JJA are up to 1.2 W m^{-2}, as listed in Table 2. The enhancement of solar absorption by the existence of aerosol above cloud has been shown to be important by *Haywood and Boucher* [2000]. The downward solar flux has experienced less water vapor attenuation above clouds. Therefore, the BC absorption is stronger for a larger downward solar flux. The cloud reflection can also enhance the solar absorption by BC, since the solar photon path length is increased due to the multiple scattering caused by the reflection. The probability of absorption of a photon increases with a longer photon path length. There are large regions with nonsignificant changes in the Northern Hemisphere in JJA. Thus, the result of BC absorption above clouds has larger year-to-year variation compared with that of BC absorption in the clouds.

[41] Table 2 also lists changes in solar reflected upward flux at TOA (FSR) and changes in solar downward flux at the surface (FSG). In STAD-NOCL, changes in FSR are negative for global and hemispheric means. The enhancement of atmospheric absorption causes a decrease in FSR. In addition, the reduced cloud amount is associated with reductions in FSR, since the cloud albedo is generally much larger than the surface albedo. In STAD-NOUP, changes in FSR are also negative. Therefore, BC leads to net warming in the atmosphere regardless of where the BC particles are located.

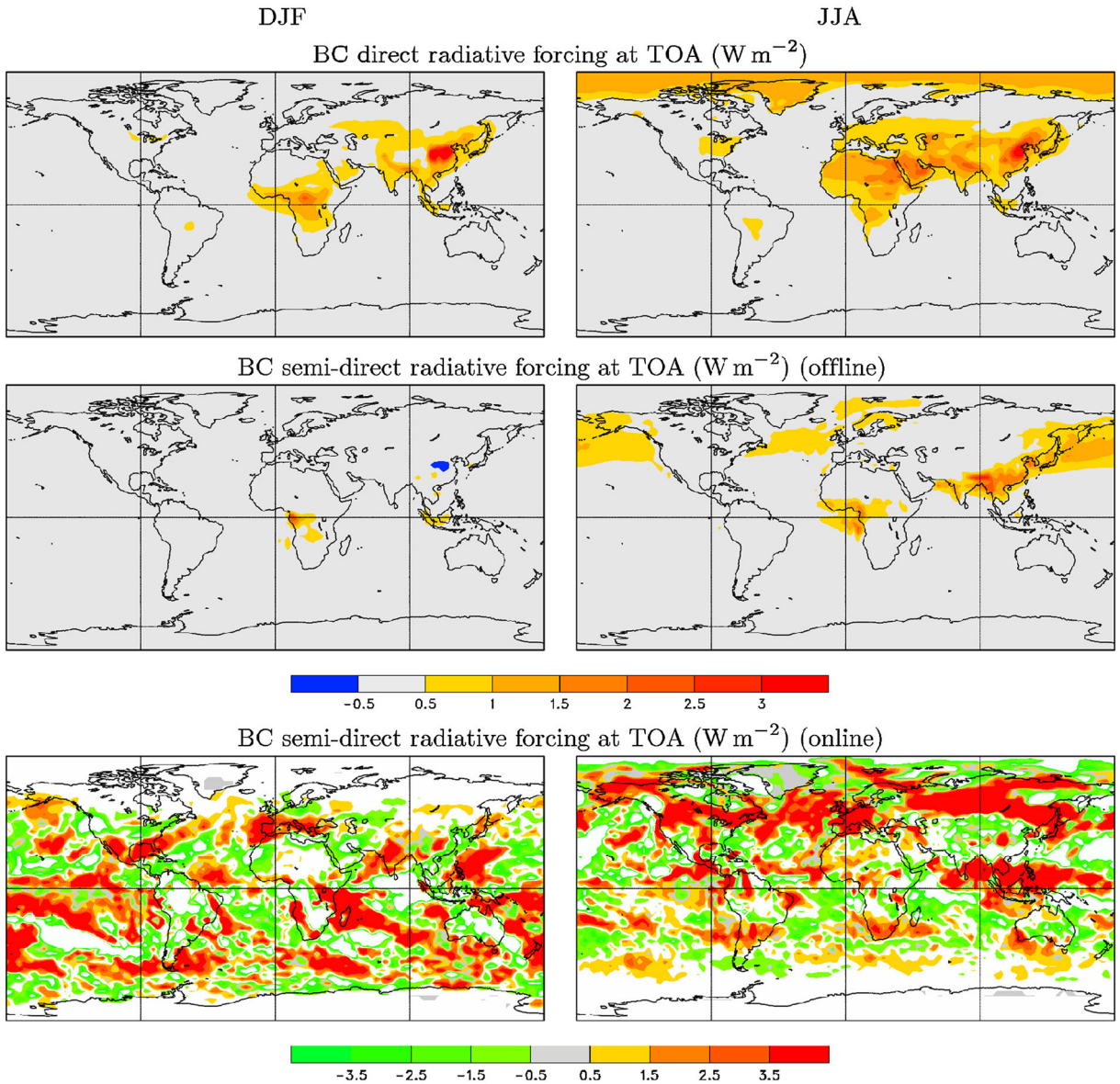

Figure 10. (top row) BC direct radiative forcing at TOA, (middle row) offline semi-direct forcing, and (bottom row) online semi-direct forcing.

[42] In STAD-NOCL, reductions in cloud amount cause an increase in FSG, due to reduced cloud reflection. In Table 2, it is clearly shown that the total change in FSA + FSR + FSG is close to zero for the global mean and hemispheric mean, because of energy conservation. For STAD-NOUP, the increase in FSA is relatively large, and the decrease in CLDT is generally smaller than for STAD-NOCL. The change in FSG becomes negative due to the near-balance of FSA, FSR, and FSG.

4. Semi-Direct Forcing

[43] Radiative forcings are often calculated as instantaneous forcings. In order to diagnose instantaneous forcings in STAD, the radiation code is executed twice at each time step. The first calculation accounts for all aerosol effects, as described for simulation STAD above. In the second radiation calculation, concentrations of BC are set to zero in the radiation code. The difference in net radiative flux between the two calculations is called the total instantaneous radiative forcing due to BC.

$$\mathrm{TRF} = F_{\mathrm{BC}} - F_{\mathrm{NBC}} ,$$

where F_{BC} and F_{NBC} are the all sky net radiative fluxes at TOA with and without BC.

[44] The instantaneous clear-sky aerosol direct radiative forcing is

$$\mathrm{DRF} = F^{\mathrm{clr}}_{\mathrm{BC}} - F^{\mathrm{clr}}_{\mathrm{NBC}} ,$$

where $F^{\mathrm{clr}}_{\mathrm{BC}}$ and $F^{\mathrm{clr}}_{\mathrm{NBC}}$ are the clear-sky net radiative fluxes at TOA with and without BC. In Figure 10 (top row), the BC direct radiative forcing at TOA is shown. The BC direct forcing is highly correlated to the loading of BC as shown in Figure 3.

[45] The BC direct radiative forcing is positive (warming effect) in all regions. This is different from other aerosols,

Table 3. The BC Direct and Semi-Direct Radiative Forcing at TOA for Global Mean (Globe) and Northern Hemisphere Mean (North) and Southern Hemisphere (South) (in Units of 10^{-1} W m^{-2})

	Direct Forcing			Semi-direct Forcing (Offline)			Semi-direct Forcing (Online)		
	Globe	North	South	Globe	North	South	Globe	North	South
Annual	2.64	4.59	1.35	1.32	1.84	0.985	2.13	0.191	2.01
DJF	1.94	2.55	1.53	0.794	0.482	1.00	1.77	0.839	2.39
JJA	2.93	5.67	1.11	1.92	3.48	0.888	2.51	3.07	1.70

which generally produce negative direct radiative forcing (cooling effect). As mentioned above, BC causes efficient absorption but relatively little scattering. Thus, an increase BC generally leads to less reflection at TOA.

[46] The BC semi-direct radiative forcing at TOA from BC inclusions in cloud droplets is shown in Figure 10 (middle row), which is obtained by subtracting the direct radiative forcing from the total instantaneous radiative forcing. This type of semi-direct forcing only represents part of the change in the net flux since the burn-off of clouds is not considered in this calculation. *Wang* [2004] called this forcing the offline semi-direct forcing.

$$\begin{aligned} \mathrm{SRF} &= \mathrm{TRF} - \mathrm{DRF} \\ &= F_{\mathrm{BC}} - F_{\mathrm{NBC}} - \left(F_{\mathrm{BC}}^{\mathrm{clr}} - F_{\mathrm{NBC}}^{\mathrm{clr}}\right) \\ &= (F_{\mathrm{BC}} - F_{\mathrm{BC}}^{\mathrm{clr}}) - \left(F_{\mathrm{NBC}} - F_{\mathrm{NBC}}^{\mathrm{clr}}\right) . \end{aligned} \tag{1}$$

In general, the offline BC semi-direct radiative forcing is also positive. However, there is a negative area in northeastern China, which is counterintuitive given that BC acts to increase the absorption of solar radiation in cloud droplets. Negative values can be attributed to the calculation method that is used for the direct radiative forcing. In completely overcast regions, the assumption of clear-sky conditions in diagnostic calculations of radiative forcings is not meaningful. Therefore, the total instantaneous forcing is generally smaller than the direct forcing. For example, if BC is located near the surface, clouds tend to attenuate the solar beam which results in less radiative forcing compared to assumed clear-sky condition. It is noted that much of the BC in northeastern China tends to occur at relatively low levels in the atmosphere.

[47] In the last equation of equation (1), $F_{\mathrm{BC}} - F_{\mathrm{BC}}^{\mathrm{clr}}$ is the cloud radiative forcing with BC included and $F_{\mathrm{NBC}} - F_{\mathrm{NBC}}^{\mathrm{clr}}$ is the cloud radiative forcing with BC excluded. Therefore, the semi-direct forcing can also be understood as the change in cloud radiative forcing due to BC. This gives a new meaning to the semi-direct effect. As discussed in previous sections, BC inclusions in cloud droplets can cause changes in cloud fraction and water path. These changes can affect the cloud radiative forcing. However, for the instantaneous result, the cloud fraction and water path do not respond to changes in BC concentrations. We therefore perform another 11 year climate integration based on STAD in which BC aerosol are not radiatively activated. We refer to this simulation as NOAL. By calculating differences in TOA cloud radiative fluxes between NOAL and STAD, we obtain the BC semi-direct forcing which accounts for all contributions of BC to cloud radiative fluxes. *Wang* [2004] called this forcing the online semi-direct forcing. In Figure 10 (bottom row), distributions of online semi-direct forcing at TOA are shown. Because of cloud and circulation feedbacks, patterns of the semi-direct forcing are more complicated and are less directly related to the location of BC aerosols compared to the offline results. There are many regions with negative forcing values. In regions with low solar incoming radiation such as for high latitude regions in DJF, the confidence level according to the *t* test is relatively low.

[48] Table 3 lists global and hemispheric means of BC direct and semi-direct forcings. The global annual mean BC direct forcing is 0.264 W m^{-2}. A review of current model estimates of black carbon radiative effects provides a direct radiative forcing of +0.33 W/m^2 [*Feichter and Stier*, 2012]. It has been previously shown that the aerosol direct forcing is approximately proportional to the aerosol loading [*Li et al.*, 2008]. As mentioned above, the BC loading in CanAM4 is slightly lower than the corresponding model median value from AeroCom which partly explains the somewhat weaker radiative forcing in CanAM4.

[49] The global annual mean offline semi-direct forcing is 0.132 W m^{-2}, which is about half of the direct radiative forcing. The global annual mean online semi-direct forcing is 0.230 W m^{-2}. Results of semi-direct forcings at TOA from other models are summarized in *Koch and Del Genio* [2010]. A wide range of positive and negative forcings were reported. As pointed by *Koch and Del Genio* [2010], reductions (enhancements) in low to middle level cloud fractions have a positive (negative) net radiative effect, which causes net warming (cooling). According to results of our study, absorption of solar radiation by BC inclusions in cloud droplets leads to a reduction in total cloud amounts. Since the cloud albedo is much larger than the surface albedo, the simulated reduction in cloud amounts leads to a reduction in reflection of solar radiation and a positive radiative forcing. As was shown above, BC inclusions in cloud droplets considerably enhance the overall BC warming effect compared to interstitial BC. This leads to a global mean positive radiative forcing. In both hemispheres, the variation in online diagnosed semi-direct forcing is larger than the corresponding offline result.

5. Conclusion

[50] The semi-direct effect refers to responses of clouds and climate to extra heating from absorption of solar radiation by BC aerosols in or near clouds [*Hansen et al.*, 1997]. However, contributions of BC inclusions in cloud droplets to the semi-direct effect have received little attention in the scientific literature. Since most of the BC aerosol particles are hydrophilic, an omission of these contributions is problematic with regard to accurate simulations of cloud optical properties. *Li et al.* [2011] previously proposed a

perturbation method to account for changes in cloud optical properties by BC inclusions in cloud droplets. Here, this parameterization was applied to study the BC semi-direct effect in CanAM4.

[51] According to simulations with CanAM4, the BC volume mixing ratio in cloud water, η, is within the range of $10^{-6} - 10^{-8}$. It is generally high in the Arctic in winter due to low cloud water content and high BC concentrations. η tends to be much lower in the tropics due to a relatively high cloud water content in the tropics.

[52] Black carbon inclusions in cloud droplets cause increases in cloud amounts in some regions and decreases in other regions. The global annual total cloud amount decreases slightly by –0.023%. However changes in cloud amounts are over 10% in some regions. A substantial latitudinal variation in the response of the cloud fractions to BC inclusions is found. Changes in cloud fraction and vertical velocity are generally well correlated. Regions with increasing cloud fraction tend to be associated with increased upward air motion. Therefore, cloud fraction changes are related to changes in vertical velocity from additional heating by absorption of solar radiation by BC. Cloud evaporation due to the additional heating plays a substantial role for changes in cloud amount. Generally, effects of BC are more clearly seen in changes in cloud water mixing ratio (path) because the net changes are less affected by contributions from high clouds. Changes in cloud water mixing ratio are particularly large in the tropics and at midlatitudes. Results also provide evidence that BC above clouds tends to stabilize the atmosphere and therefore enhances the cloud fraction in the atmospheric boundary layer.

[53] Relationships between aerosol optical depth and cloud amounts based on satellite data are consistent with radiative effects of BC above cloud base. In regions of relatively high BC loading, concentrations of BC above cloud top also tend to be high. Additional heating above clouds from absorption of solar radiation by BC tends to stabilize the atmosphere and therefore causes increases in amounts of boundary layer clouds. On the other hand, concentrations of BC above clouds tend to be lower in regions of low BC loading. For clouds in these regions, the extra heating from BC inclusions in cloud droplets causes the clouds to burn off more efficiently relative to the stabilizing effect of BC above cloud top.

[54] The global mean enhancement of solar absorption is about 0.0485 W m^{-2} for BC inclusions in cloud droplets. On the other hand, BC above clouds causes an enhancement of 0.571 W m^{-2}.

[55] The BC semi-direct radiative forcing can be obtained by subtracting the direct radiative forcing from the total radiative forcing. It is found that the online BC semi-direct forcing at TOA is generally comparable to the direct radiative forcing. The BC online semi-direct forcing is mostly positive, which further enhances the BC warming effect.

[56] *Yue et al.* [2011] found that feedbacks involving changes in sea surface temperatures are important for the local dust aerosol forcing. However, climate feedbacks involving ocean responses are not considered in the present study. Simulations with coupled climate models are useful for studies of feedbacks between BC and climate [*Wang et al.*, 2013].

[57] It is interesting that feedbacks resulting from BC warming can lead to changes in high altitude ice clouds. Inclusions of BC in ice cloud particles were not considered in this study and therefore changes for ice clouds were not analyzed in detail here. BC potentially plays an important role for ice cloud microphysics, particularly in mixed-phase clouds that are part liquid and part ice. In these clouds, BC may act as ice nuclei that enhance ice formation and increase ice fallout [*Bond et al.*, 2013].

[58] **Acknowledgments.** The authors would like to thank J. Cole, Editor S. Ghan, and three anonymous reviewers for constructive comments. The authors acknowledge the Interagency Monitoring of Protected Visual Environments (IMPROVE) program, Global Atmospheric Watch (GAW), and European Monitoring and Evaluation Programme (EMEP) for providing measurement data for black carbon. H. Zhang was supported by the National Basic Research Program of China (2011CB403405), and X.-Z. Liang was supported by the U.S. USEPA grant (20110150701).

References

Baumer, D., U. Lohmann, G. Lesins, J. Li, and B. Croft (2007), Parameterization of the optical properties of carbonaceous in the Canadian Center for Climate Modelling and Analysis AGCM with impact on global radiation and energy fluxes, *J. Geophys. Res.*, *112*(D10207), 4564, doi:10.1029/2006JD007319.

Bond, T. C., et al. (2013), Bounding the role of black carbon in the climate system: A scientific assessment, *J. Geophys. Res.*, doi:10.1002/jgrd.50171.

Briegleb, B. P. (1992), delta-Eddington approximation for solar radiation in the NCAR community climate model, *J. Geophys. Res.*, *97*, 7903–7612.

Brioude, J., et al. (2009), Effect of biomass burning on marine stratocumulus clouds off the California coast, *Atmos. Chem. Phys.*, *9*, 8841–8856, doi:10.5194/acp-9-8841-2009.

Croft, B., U. Lohmann, and K. von Salzen (2005), Black carbon ageing in the Canadian Centre for Climate Modelling and Analysis atmospheric general circulation model, *Atmo. Chem. Phys.*, *5*(7), 1931–1949.

Chuang, C. C., J. E. Penner, J. M. Prospero, K. E. Grant, G. H. Rau, and K. Kawamoto (2002), Cloud susceptibility and the first aerosol indirect forcing: Sensitivity to black carbon and aerosol concentrations, *J. Geophys. Res.*, *107*(D21), 4564, doi:10.1029/2000JD000215.

Chung, S. H., and J. H. Seinfeld (2005), Climate response of direct radiative forcing of anthropogenic black carbon, *J. Geophys. Res.*, *110*, D11102, doi:10.1029/2004JD005441.

Chylek, P., G. B. Lesins, G. Videen, J. G. D. Wong, R. G. Pinnick, D. Ngo, and J. D. Klett (1996), Black carbon and absorption of solar radiation by clouds, *J. Geophys. Res.*, *101*, 23,365–23,371, doi:10.1029/96JD01901.

Dentener, F., et al. (2006), Emissions of primary aerosol and precursor gases in the years 2000 and 1750 prescribed data sets for AeroCom, *Atmos. Chem. Phys.*, *6*, 4321–4344.

Flossmann, A. (1998), Interaction of aerosol particles and clouds, *J. Atmos. Sci.*, *55*, 879–887.

Feichter, J., and P. Stier (2012), Assessment of black carbon radiative effects in climate models, *Wiley Interdisciplinary Reviews: Climate Change*, *3*(4), 359–370.

Flossmann, A., and W. Wobrock (2010), A review of our understanding of the aerosol-cloud interaction from the perspective of a bin resolved cloud scale modelling, *Atmos. Res.*, *97*, 478–497.

Ghan, S. J., X. Liu, R. C. Easter, R. Zaveri, P. J. Rasch, and J.-H. Yoon (2012), Toward a minimal representation of aerosols in climate models: Comparative decomposition of aerosol direct, semi-direct and indirect radiative forcing, *J. Clim.*, *25*, 6461–6476.

Gustafson, W. I., Jr., L. K. Berg, R. C. Easter, and S. J. Ghan (2008), The explicit-cloud parameterized-pollutant hybrid approach for aerosol-cloud interactions in multiscale modeling framework models: Tracer transport results, *Environ. Res. Lett.*, *3*, 025005, doi:10.1088/1748-9326/3/2/025005.

Hansen, J., M. Sato, and R. Ruedy (1997), Radiative forcing and climate response, *J. Geophys. Res.*, *102*, 6831–6864.

Hansen, J., et al. (2005), Efficacy of climate forcings, *J. Geophys. Res.*, *110*, D18104, doi:10.1029/2005JD005776.

Haywood, J., and O. Boucher (2000), Estimates of the direct and indirect radiative forcing due to tropospheric aerosols: A review, *J. Geophys. Res.*, *38*, 513–543.

Hill, A. A., and S. Dobbie (2008), The impact of aerosols on nonprecipitating marine stratocumulus. II: The semi-direct effect, *Q. J. Roy. Meteor. Soc.*, *134*(634), 1155–1165, doi:10.1002/qj.277.

Jacobson, M. Z. (2006), Effects of absorption by soot inclusions within clouds and precipitation on global climate, *J. Phys. Chem.*, *110*, 6860–6873.

Johnson, B. T., K. P. Shine, and P. M. Forster (2004), The semidirect aerosol effect: Impact of absorbing aerosols on marine stratocumulus, *Q. J. Roy. Meteor. Soc.*, *130*(599), 1407–1422, doi:10.1256/qj.03.61.

Jones, A., J. M. Haywood, and O. Boucher (2007), Aerosol forcing, climate response and climate sensitivity in the Hadley Centre climate model, *J. Geophys. Res.*, *112*, D20211, doi:10.1029/2007JD008688.

Koch, D., and A. D. Del Genio (2010), Black carbon semi-direct effects on cloud cover: Review and synthesis, *Atmos. Chem. Phys.*, *10*, 7685–7696.

Koch, D., et al. (2009), Evaluation of black carbon estimations in global aerosol models, *Atmos. Chem. Phys.*, *9*, 9001–9026.

Koren, I., Y. J. Kaufman, L. A. Remer, and J. V. Martins (2004), Measurement of the effect of Amazon smoke on inhibition of cloud formation, *Science*, *303*, 1342–1345.

Li, J., and H. W. Barker (2005), A radiation algorithm with correlated k-distribution. Part I: Local thermal equilibrium, *J. Atmos. Sci.*, *62*, 286–309.

Li, J., X. Ma, K. von Salzen, and S. Dobbie (2008), Parameterization of sea salt optical properties and related radiative forcing study, *Atmos. Chem. Phys.*, *8*, 4787–4798.

Li, J., E. Mlawer, and P. Chylek (2011), Parameterization of cloud optical properties for semidirect radiative forcing, *J. Geophys. Res.*, *116*, D23212, doi:10.1029/2011JD016611.

Perlwitz, J., and R. L. Miller (2010), Cloud cover increase with increasing aerosol absorptivity? A counterexample to the conventional semi-direct aerosol effect, *J. Geophys. Res*, *115*, D08203, doi:10.1029/2009JD012637.

Räisänen, P., H. W. Barker, M. Khairoutdinov, J. Li, and D. Randall (2004), Stochastic generation of subgrid-scale cloudy columns for large-scale models, *Q. J. R. Meteor. Soc.*, *130*, 2047–2068.

Ten Hoeve, J. E., L. A. Remer, and M. Z. Jacobson (2011), Microphysical and radiative effects of aerosols on warm clouds during the Amazon biomass burning season as observed by MODIS: Impacts of water vapor and land cover, *Atmos. Chem. Phys.*, *11*, 3021–3036.

Torseth, K., W. Aas, K. Breivik, A. M. Fjaoaa, M. Fiebig, A. G. Hjellbrekke, C. Lund Myhre, S. Solberg, and K. E. Yttri (2012), Introduction to the European Monitoring and Evaluation Programme (EMEP) and observed atmospheric composition change during 1972–2009, *Atmos. Chem. Phys.*, *12*, 5447–5481.

von Salzen, K., et al. (2013), The Canadian fourth generation atmospheric global climate model (CanAM4). Part I: Physical processes, *Atmosphere Ocean*, *51*, 104–125, doi:10.1080/070559002012.755610.

Wang, C. (2004), A modeling study on the climate impacts of black carbon aerosols, *J. Geophys. Res.*, *109*, D03106, doi:10.1029/2003JD004084.

Wang, Z., H. Zhang, J. Li, X. Jing, and P. Lu (2013), Radiative forcing and climate response due to the presence of black carbon in cloud droplets, *J. Geophys. Res.*, *118*, doi:10.1002/jgrd.50312.

Yoshimori, M., and A. J. Broccoli (2008), Equilibrium response of an atmosphere-mixed layer ocean model to different radiative forcing agents: Global and zonal mean response, *J. Clim.*, *21*, 4399–4423.

Yue, X., H. Liao, H. J. Wang, S. L. Li, and J. P. Tang (2011), Role of sea surface temperature responses in simulation of the climatic effect of mineral dust aerosol, *Atmos. Chem. Phys.*, *11*(12), 6049–6062, doi:10.5194/acp-11-6049-2011.

Zhang, H., Z.-L. Wang, P.-W. Guo, and Z.-Z. Wang (2009), A modeling study of the effects of direct radiative forcing due to carbonaceous aerosol on the climate in East Asia, *Adv. Atmos. Sci.*, *26*(1), 1–10.

Zhuang, B. L., L. Liu, F. H. Shen, T. J. Wang, and Y. Han (2010), Semidirect radiative forcing of internal mixed black carbon cloud droplet and its regional climatic effect over China, *J. Geophys. Res.*, *115*, D00K19, doi:10.1029/2009JD013165.